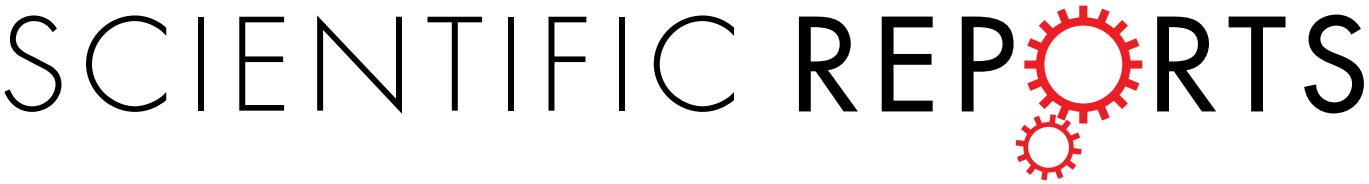

OPEN

An application of $(4YSZ)_{0.93}(Fe_2O_3)_{0.07}$ in limiting current oxygen sensor

Received: 17 May 2018
Accepted: 13 December 2018
Published online: 05 April 2019

Xiangnan Wang, Tao Liu & Jingkun Yu

$(4YSZ)_{0.93}(Fe_2O_3)_{0.07}$ and 9 mol% Y_2O_3 stabilized ZrO_2 (9YSZ) were synthesized by co-precipitation method and their crystalline structure, microstructure, electronic conductivity, total conductivity were characterized. A limiting current oxygen sensor was assembled with $(4YSZ)_{0.93}(Fe_2O_3)_{0.07}$ dense diffusion barrier and 9YSZ solid electrolyte by Pt sintered-paste method. Influences of temperature (T), oxygen concentration ($x(O_2)$) and water vapor pressure ($p(H_2O)$) on sensing characteristics of the limiting current oxygen sensor were investigated. The crystalline structure of $(4YSZ)_{0.93}(Fe_2O_3)_{0.07}$ and 9YSZ belong to cubic structure with $Fm\bar{3}m$. The total conductivity of $(4YSZ)_{0.93}(Fe_2O_3)_{0.07}$ is higher than that of 9YSZ and the electronic and total conductivities of the samples meet the linear relationship with 1000/T. The limiting current oxygen sensor exhibits excellent sensing characteristics under test conditions. The effects of T, $x(O_2)$ and $p(H_2O)$ are as follows: $Log(I_L \cdot T)$ depends linearly on 1000/T, I_L depends linearly on $x(O_2)$ and I_L is not significantly dependent on $p(H_2O)$.

It is essential to control the air-fuel ratio (A/F) to increase fuel economy and decrease environmental pollution since industrial furnaces and automobile industry expend immense amounts of energy. Solid electrolyte oxygen sensors play an important role for detecting the oxygen concentration in exhaust gas. Solid electrolyte oxygen sensors include two types: galvanic cell type and limiting current type. Potential of galvanic cell oxygen sensor is a function of logarithm of oxygen concentration ratio, causing the sensor to be less sensitive at high oxygen concentration. Limiting current of limiting current oxygen sensors is directly a linear function of oxygen concentration, resulting in the measurement range to be higher accuracy[1]. Limiting current oxygen sensors consist of three types: aperture type, porous type and dense diffusion barrier type. Early researches focused on aperture and porous types limiting current oxygen sensors, but unfortunately, there are some problems, such as pores are easily blocked and porous porosity is difficult to control. These weaknesses restrict the application of aperture and porous types limiting current oxygen sensors. In contrast, limiting current oxygen sensor with mixed ionic-electronic conducting oxides (MIECs) as dense diffusion barrier has been widely concerned by overcoming the shortcomings of the two previous limiting current oxygen sensors[2]. At the same time, the study of MIECs has also attracted the attention of researchers due to its widely application in gas sensors, solid oxide fuel cell and oxygen separation membranes at high temperatures[3–5]. YSZ is an excellent solid electrolyte due to its outstanding chemical stability, physical stability and oxide ionic conductivity[6–8]. Many researches were conducted on dense diffusion barrier limiting current oxygen sensor with different MIECs as dense diffusion barrier and YSZ solid electrolyte[9–12]. Peng *et al.*[9] developed a sensor with Pt-YSZ composite as dense diffusion barrier. The results showed that the sensor had a limiting current plateau for $x(O_2)$ up to 6% and the I_L depended linearly on $x(O_2)$. Xia *et al.*[10] developed a sensor with $La_{0.8}Sr_{0.2}MnO_3$ (LSM) as dense diffusion barrier by Pt sintered-paste method. The results showed that the method can avoid the mismatch of shrinkage between two kinds of LSM and YSZ materials during sintering and can provide a limiting current plateau in a full range of air-fuel ratio. Shi *et al.*[11] developed a sensor with LSM-YSZ composite as dense diffusion barrier by co-pressing and co-sintering method. The results showed that the sensor exhibited a quite low operating temperature. At 400 °C, the limiting current plateau appeared in voltages of 0.7–1.2 V and it showed a good linear relationship with $x(O_2)$ up to 10%. Wang *et al.*[12] developed a sensor with $La_{0.8}Sr_{0.2}FeO_3$ (LSF) as dense diffusion barrier. The results showed that the sensor exhibited a performance in oxygen concentrations range of 0–21%. In the above researches, YSZ is solid electrolyte, while the dense diffusion barrier materials have the problem of high cost or mismatch with YSZ solid electrolyte. Fe_2O_3 is a transition metal oxide and Fe^{3+} will redox at different oxygen concentration to form redox

School of Metallurgy, Northeastern University, Shenyang, Liaoning, 110819, China. Correspondence and requests for materials should be addressed to T.L. (email: liut@smm.neu.edu.cn)

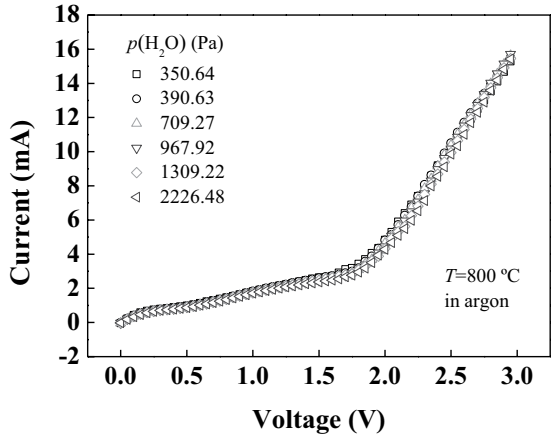

Figure 1. The cross section of dense diffusion barrier limiting current oxygen sensor.

Fe^{3+}/Fe^{2+} couple. Doping Fe_2O_3 into YSZ can make the material have electronic and ionic conductivity. On the other hand, Fe_2O_3 doped YSZ has good chemical compatibility with YSZ solid electrolyte at elevated temperature. The research on doping Fe_2O_3 into YSZ to get MIEC as dense diffusion barrier has not reported yet.

In this paper, $(4YSZ)_{0.93}(Fe_2O_3)_{0.07}$ and 9YSZ were synthesized by co-precipitation method and their crystalline structure, microstructure, electronic conductivity, total conductivity were characterized, respectively. A limiting current oxygen sensor with $(4YSZ)_{0.93}(Fe_2O_3)_{0.07}$ as dense diffusion barrier and 9YSZ solid electrolyte was developed by Pt sintered-paste method. The effects of T, $x(O_2)$ and $p(H_2O)$ were studied, respectively.

Experimental

$(4YSZ)_{0.93}(Fe_2O_3)_{0.07}$ and 9YSZ powders were synthesized by co-precipitation method. The analytical reagents $Y(NO_3)_3{\cdot}6H_2O$ (purity 99.99%), $ZrOCl_2{\cdot}8H_2O$ (purity 99.9%), $FeCl_3{\cdot}6H_2O$ (purity 99%) and $NH_3{\cdot}H_2O$ (purity 0.1 M) were purchased from Aladdin (www.aladdin-e.com) and used directly without further purification. First, reagents $Y(NO_3)_3{\cdot}6H_2O$, $ZrOCl_2{\cdot}8H_2O$ and $FeCl_3{\cdot}6H_2O$ were weighed according to stoichiometry and dissolved in homemade distilled water with intense stirring. Second, reagent $NH_3{\cdot}H_2O$ was dripped into the salt solution with continuous stirring until pH reached 9 to get precipitates. The precipitates were washed by distilled water and ethanol for two times, respectively, and then dried at 70 °C for 12 h to obtain precursor powders. Thirdly, the precursor powders were calcined at 800 °C for 12 h to obtain solid solution powders. Crystalline structure of the solid solution powders was characterized by X-ray diffraction (Philips 3040/60, Netherlands, www.usa.philips.com, Cu Kα, 40 mA, 40 kV) and the data were refined and calculated by GSAS software[13]. We pressed the solid solution powders and then sintered it at 1600 °C for 10 h in air to obtain the samples for measurement of electrical conductivity, microstructure and sensors. Electronic and total conductivities were measured by Hebb-Wagner and DC van der Pauw methods, respectively. Microstructure of the samples on the cross-section was observed by scanning electron microscopy (Ultra Plus, Germany, www.zeiss.com.cn). A limiting current oxygen sensor was prepared by Pt sintered-paste method with $(4YSZ)_{0.93}(Fe_2O_3)_{0.07}$ dense diffusion barrier and 9YSZ solid electrolyte. Pt paste (www.guyou01.com.cn) was screen printed on the top and bottom of the 9YSZ solid electrolyte as an electrode, Pt wire (Diameter 0.1 mm, China, www.reagent.com.cn) connected to the electrode as a lead. The sintered $(4YSZ)_{0.93}(Fe_2O_3)_{0.07}$ sample was attached to the top of the sintered 9YSZ sample with Pt paste and heated at 800 °C for 1 h to obtain a dense diffusion barrier limiting current oxygen sensor. The Pt layer between $(4YSZ)_{0.93}(Fe_2O_3)_{0.07}$ and 9YSZ is to connect them together and the sides of the sample were sealed with glass glaze (www.sic.ac.cn). The cross section of the sensor is shown in Fig. 1 (not to scale).

The effects of T, $x(O_2)$ and $p(H_2O)$ on the I-V characteristics of the sensor were studied, and data were measured by an electrochemical analysis system (LK98B II, China, lanlike.b2b.hc360.com). Limiting current plateau was obtained at temperatures in the order of 800–650 °C and in the oxygen concentration region of 2–7%. By adjusting the temperature of the $LiCl{\cdot}H_2O$ saturated solution to control the water vapor pressure in the volumetric flask, argon (Ar) was introduced into the solution to carry the water vapor into the measured furnace to obtain testing conditions of $p(H_2O)$. O_2 and Ar flow were controlled by capillary flowmeters and the total flow rate in the sensing performance experiment was about 100 ml/min. The testing system mentioned above for oxygen sensor is shown in Fig. 2.

Results and Discussion

Property of $(4YSZ)_{0.93}(Fe_2O_3)_{0.07}$ and 9YSZ. The crystalline structure of 9YSZ and $(4YSZ)_{0.93}(Fe_2O_3)_{0.07}$ belongs to cubic structure with $Fm\bar{3}m$ shown in Fig. 3(a), which is consistent with previous studies[14]. The diffraction peaks of monoclinic ZrO_2 (m-ZrO_2) in 9YSZ sample are found at 2θ of 28.32° and 31.39°, which may be due to incomplete reactions. In the $(4YSZ)_{0.93}(Fe_2O_3)_{0.07}$ sample, the diffraction peak intensity of the m-ZrO_2 at 28.32° becomes weaker and the diffraction peak intensity at 31.39° position disappears, which shows that the doping of Fe_2O_3 is more beneficial to the formation of cubic ZrO_2 (c-ZrO_2). Meanwhile, we did not find the diffraction peak of Fe_2O_3 in the sample. For comparison, we further increased the x and obtained the $(4YSZ)_{0.93}(Fe_2O_3)_{0.07}$ sample, and found the diffraction peak of Fe_2O_3, which indicating that Fe_2O_3 did not doped into YSZ. The calculated cell

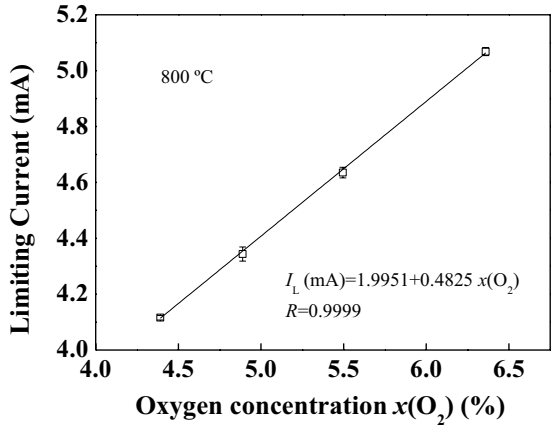

Figure 2. Diagram of testing system for oxygen sensor.

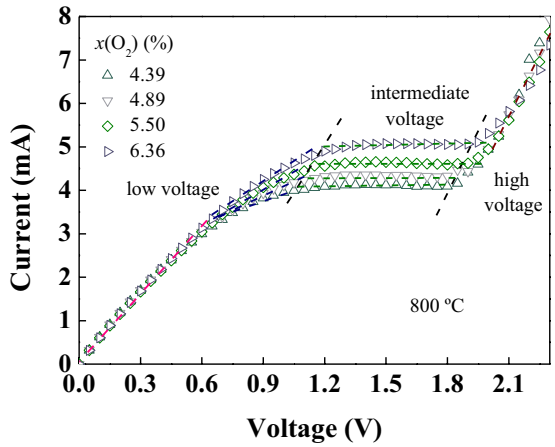

Figure 3. Crystalline structure and calculated cell parameters of the 9YSZ and $(4YSZ)_{0.93}(Fe_2O_3)_{0.07}$ samples.

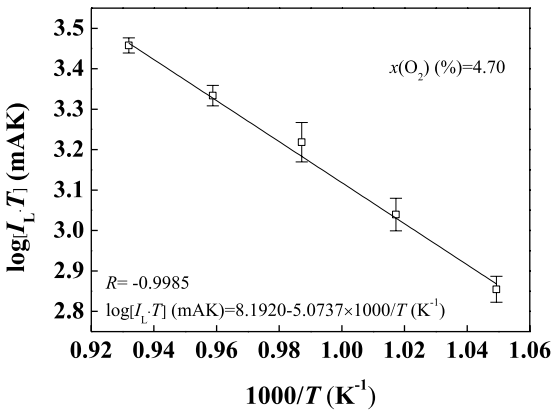

Figure 4. The microstructure of the 9YSZ and $(4YSZ)_{0.93}(Fe_2O_3)_{0.07}$ samples on the cross-section.

parameters of samples are shown in Fig. 3(b), it is found that the cell parameters reduced from 5.130209 of the YSZ samples to 5.123664 of the $(4YSZ)_{0.93}(Fe_2O_3)_{0.07}$ samples and the cell volume reduced from 135.022 to 134.506, indicating that Fe_2O_3 is doped into YSZ. This decrease of the cell parameters is due to the substitution of smaller Fe^{3+} ions (0.055 nm) in YSZ for Zr^{4+} ions (0.084 nm)[15,16].

The microstructure of the 9YSZ and $(4YSZ)_{0.93}(Fe_2O_3)_{0.07}$ samples on the cross-section is shown in Fig. 4. It can be seen from the diagram that the grains of the 9YSZ sample can be seen clearly and evenly distributed, and the grains of the $(4YSZ)_{0.93}(Fe_2O_3)_{0.07}$ sample are closely linked together, and the samples are dense. The total

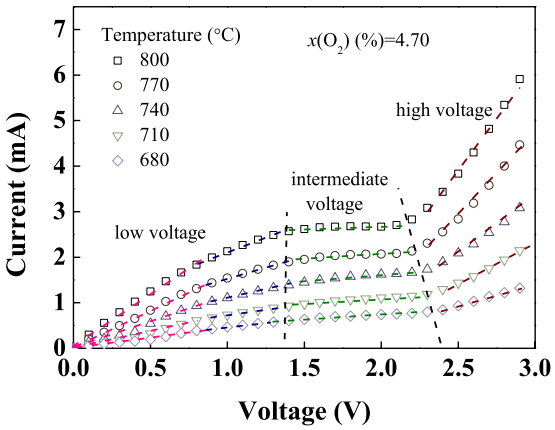

Figure 5. The electrical conductivity of the 9YSZ and $(4YSZ)_{0.93}(Fe_2O_3)_{0.07}$ samples.

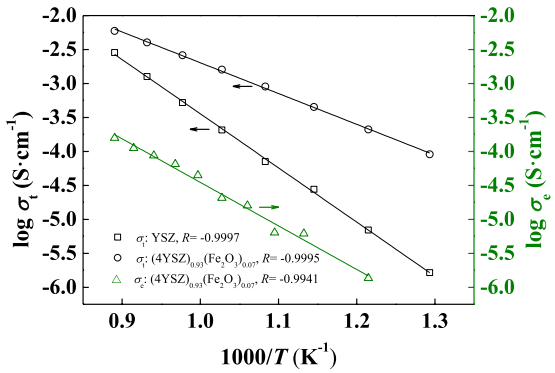

Figure 6. *I-V* characteristic curves of the oxygen sensor in different temperature in an oxygen concentration of 4.70%.

conductivity of the 9YSZ and $(4YSZ)_{0.93}(Fe_2O_3)_{0.07}$ samples and the electronic conductivity of $(4YSZ)_{0.93}(Fe_2O_3)_{0.07}$ sample are shown in Fig. 5. The total conductivity of $(4YSZ)_{0.93}(Fe_2O_3)_{0.07}$ is higher than that of the YSZ sample. The total and electronic conductivity of the samples meet the linear relationship with the temperature.

Effect of temperature on the sensor. *I-V* characteristic curves of the oxygen sensor with $(4YSZ)_{0.93}(Fe_2O_3)_{0.07}$ dense diffusion barrier in the temperature range of 800–680 °C in an oxygen concentration of 4.70% are shown in Fig. 6. It can be seen that from the pattern that the *I-V* characteristic curves of the sensor are mainly divided into three regions, which are located in low voltage region, intermediate voltage region and high voltage region, respectively, and the dashed lines representing a linear fit to the data. (1) In low voltage region, output current increases linearly with increasing applied voltage, which is predominantly caused by ohmic behavior of solid electrolyte[17]. Since the conductivity of the solid electrolyte increases with increasing temperature, the slope of the ohmic section at high temperature is higher than that at low temperature. At the end of the region, the slope of ohmic behavior has a slight decrease, which may be in a transitional area. (2) In intermediate voltage region, when the pump oxygen rate of the solid electrolyte is equal to the oxygen diffusion rate of the dense diffusion barrier, the *I-V* relationship approaches a limiting current plateau, which is a valuable experimental data. The limiting current I_L of the sensor increases with increasing T, which is due to the increase of conductivity of $(4YSZ)_{0.93}(Fe_2O_3)_{0.07}$ dense diffusion barrier. (3) In high voltage, output current increases with applied voltage, which is caused by oxide reductions of solid electrolyte[18,19].

The relationship between $\log(I_L \cdot T)$ and $1000/T$ is shown in Fig. 7. The linear correlation coefficient R is −0.9985. In addition, the activation energy of the oxygen ion in the $(4YSZ)_{0.93}(Fe_2O_3)_{0.07}$ dense diffusion barrier can be calculated according to the fitting line, which is 0.9 eV in ref.[20].

Effect of oxygen concentration on the sensor. *I-V* characteristic curves of the sensor with $(YSZ)_{0.93}(Fe_2O_3)_{0.07}$ dense diffusion barrier at different oxygen concentrations are shown in Fig. 8. It can be seen that the distinct limiting current plateau is observed at oxygen concentrations of 4.3–6.4%. At high temperatures, oxygen is adsorbed on the outside of the $(4YSZ)_{0.93}(Fe_2O_3)_{0.07}$ dense diffusion barrier and the adsorbed oxygen forms oxygen ions by absorbing two electrons at the $(4YSZ)_{0.93}(Fe_2O_3)_{0.07}$/Pt/air three-phase boundary. Oxygen ions transported from the surface of the $(4YSZ)_{0.93}(Fe_2O_3)_{0.07}$ dense diffusion barrier to the $(4YSZ)_{0.93}(Fe_2O_3)_{0.07}$/9YSZ interfaces driven by oxygen pressure difference since the oxygen pressure of the surface is higher than that of the interfaces. Oxygen ions lose electrons becoming oxygen molecules, and then release

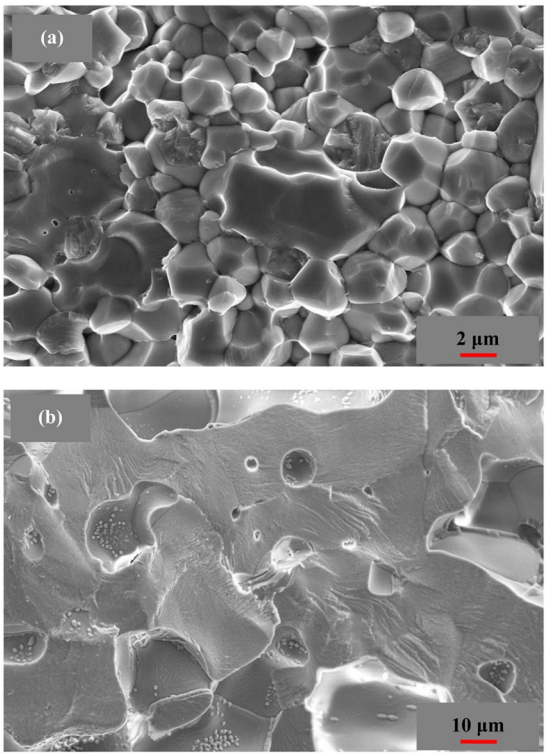

Figure 7. Relationship between $\log(I_L \cdot T)$ and $1000/T$ in an oxygen concentration of 4.70%.

oxygen. Due to the high electronic conductivity and no potential gradient of the $(4YSZ)_{0.93}(Fe_2O_3)_{0.07}$ dense diffusion barrier, oxygen ions are pressure-diffused through the dense diffusion barrier only by oxygen pressure differential between the two sides of the $(4YSZ)_{0.93}(Fe_2O_3)_{0.07}$ dense diffusion barrier. The migration rate of oxygen ions from the $(4YSZ)_{0.93}(Fe_2O_3)_{0.07}$/9YSZ interfaces to the 9YSZ solid electrolyte surface is affected by the applied voltage across solid electrolyte. The pump oxygen current rate increases with increasing applied voltage. When the pump oxygen rate of the 9YSZ solid electrolyte is equal to the oxygen diffusion rate of the $(4YSZ)_{0.93}(Fe_2O_3)_{0.07}$ dense diffusion barrier and the applied voltage increases to a certain value, the limiting current is obtained. Under lower oxygen concentration, the limiting current plateau of the sensor is obtained at lower voltage, which is consistent with results in refs[21–23].

The relationship between the limiting current and oxygen concentration at 800 °C is shown in Fig. 9. It can be seen that the limiting current and the oxygen concentration display a good linear relationship, which is related to the correlation theory of the Knudsen diffusion[24].

$$I_L = \frac{4FD_K SP}{RTL} \cdot x(O_2) \tag{1}$$

where D_K, P, T, F, R, S and L are oxygen diffusion coefficient of Knudsen diffusion, partial pressure difference of diffused gas between electrodes I and II, temperature, Faraday constant, gas constant, total cross-sectional area and length of diffusion path, respectively.

The relationship between diffusion coefficient (D_T) and temperature (T) for the solid ion diffusion mode of solid theory is as follows:

$$D_T = D_O \cdot \exp\left(-\frac{\varepsilon}{k_B T}\right) \tag{2}$$

where D_o, ε and k_B are constant of the frequency factor, activation energy for the diffusion process and the Boltzmann constant, respectively.

Combining equations (1) and (2) obtains the equation (3):

$$I_L = \frac{4FD_O SP}{RLT} \cdot x(O_2) \cdot \exp(-\varepsilon/k_B T) \tag{3}$$

If the oxygen concentration is stable, so:

$$a = \frac{4FD_O SP}{RL} x(O_2) \tag{4}$$

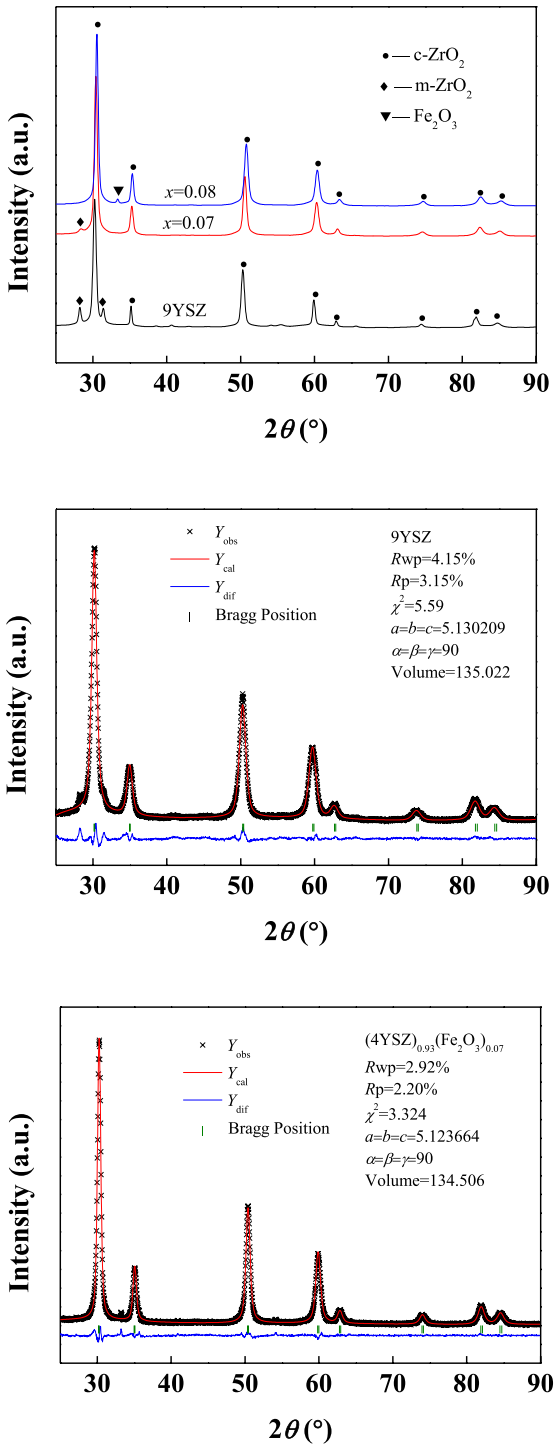

Figure 8. *I–V* characteristic curves of the sensor at different oxygen concentrations at 800 °C.

Equation (4) is brought into equation (3) to get equation (5):

$$I_L = a \cdot \frac{1}{T} \cdot \exp(-\varepsilon/k_B T) \tag{5}$$

Equation (5) becomes a logarithmic function to obtain equation (6):

$$\log I_L = A - log\ T - \frac{\varepsilon}{k_B T} \tag{6}$$

and then,

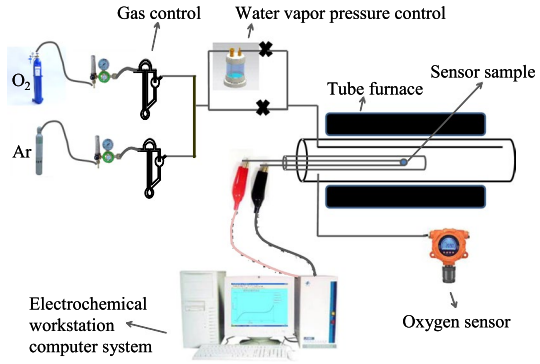

Figure 9. The relationship between the limiting current and oxygen concentration at 800 °C.

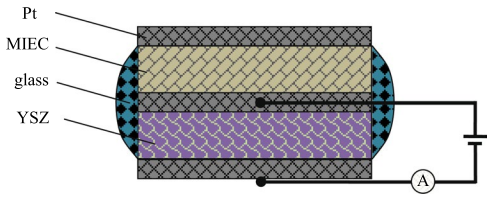

Figure 10. Relationship between *I*–*V* characteristics and water vapor pressure in an argon atmosphere at 800 °C.

$$B = -\frac{\varepsilon}{k_B} \tag{7}$$

Now, equation (6) becomes equation (8), and then becomes equation (9):

$$\log I_L = A - \log T + B \cdot \frac{1}{T} \tag{8}$$

$$\log(I_L \cdot T) = A + B \cdot \frac{1}{T} \tag{9}$$

According to equation (9), $\log(I_L \cdot T)$ and $1000/T$ have a good linear relationship at different temperatures. As shown in Fig. 8, the linear correlation between $\log(I_L \cdot T)$ and $1000/T$ is well in accordance with the Knudsen diffusion model.

Effect of water vapor pressure on the sensor. The water vapor pressure dependence of the *I*-*V* characteristics at 800 °C is shown in Fig. 10. The water vapor pressure was achieved by passing dry argon through $LiCl{\cdot}H_2O$ solution. The relationship between the water vapor pressure above saturated $LiCl{\cdot}H_2O$ solution and temperatures of 23.90–54.84 °C is known according to ref.[25]. The temperature was controlled by a constant temperature water bath. As can be seen from the figure, water vapor pressure has no obvious effect on *I*-*V* characteristics of the sensor in the measured region.

Conclusions

$(4YSZ)_{0.93}(Fe_2O_3)_{0.07}$ dense diffusion barrier was synthesized by co-precipitation method. The crystalline structure of $(4YSZ)_{0.93}(Fe_2O_3)_{0.07}$ and 9YSZ belong to cubic structure. The total conductivity of $(4YSZ)_{0.93}(Fe_2O_3)_{0.07}$ is higher than that of 9YSZ and the electrical conductivity of the samples meet the linear relationship with $1000/T$. The limiting current oxygen sensor based on $(4YSZ)_{0.93}(Fe_2O_3)_{0.07}$ dense diffusion barrier and 9YSZ solid electrolyte was developed and it demonstrated a very good linear relationship between $\log(I_L{\cdot}T)$ and $1000/T$ well in accordance with the Knudsen diffusion model. At the same time, the sensor exhibits a good sensing performance with the oxygen concentration of 4.39–6.36% at 800 °C, which also agrees with the Knudsen diffusion model. Water vapor pressure in the measured region has no obvious effect on *I*-*V* characteristics of the sensor, which means that the sensor has good selectivity for oxygen.

Data Availability

The datasets generated during and/or analysed during the current study are available from the corresponding author on reasonable request.

References

1. Wang, X. N. *et al*. Preparation and electrical property of $CaZr_{0.7}M_{0.3}O_3$ (M=Fe, Cr and Co) dense diffusion barrier for application in limiting current oxygen sensor. *Sens. Actuator B-Chem.* **266**, 455–462 (2018).
2. Liu, T. *et al*. A limiting current oxygen sensor prepared by a co-pressing and co-sintering technique. *Sens. Actuator B-Chem.* **277**, 216–223 (2018).
3. Liu, T., Li, Y. & Goodenough, J. B. $Sr_{0.7}Ho_{0.3}CoO_{3-\delta}$ as a potential cathode material for intermediate-temperature solid oxide fuel cells. *J. Power Sources* **199**, 161–164 (2012).
4. Liu, T., Zhang, X. F., Yuan, L. & Yu, J. K. A review of high-temperature electrochemical sensors based on stabilized zirconia. *Solid State Ion.* **283**, 91–102 (2015).
5. Liu, T., Zhang, X. F., Wang, X. N., Yu, J. K. & Li, L. A review of zirconia-based solid electrolytes. *Ionics* **22**, 2249–2262 (2016).
6. Stombouli, A. B. & Traversa, E. Solid oxide fuel cells (SOFCs): a review of environmentally clean and efficient source of energy. *Renew. Sustain. Energy Rev.* **6**, 433–455 (2002).
7. Blum, L., Meulenberg, W. A., Nabielek, H. & Steinberger-Wilckens, R. Worlwide SOFC technology overview and benchmark. *Int. J. Appl. Ceram. Technol.* **2**, 482–492 (2005).
8. Williams, M. C. Solid oxide fuel cells: fundamentals to systems. *Fuel Cells* **7**, 78–85 (2007).
9. Peng, Z. Y., Liu, M. L. & Balko, E. A new type of amperometric oxygen sensor based on a mixed-conducting composite membrane. *Sens. Actuator B-Chem.* **72**, 35–40 (2001).
10. Xia, H., Li, F. S., Wu, W. J., Yang, M. & Li, L. F. Limiting current oxygen sensors with LSM as dense diffusion barrier. *J. Inorg. Mater* **19**, 411–416 (2004).
11. Shi, X. & Zhang, Y. Study of YSZ amperometric oxygen sensor with a dense barrier layer. *Key Engineering Materials* **280–283**, 431–434 (2005).
12. Wang, L. *et al*. Limiting current oxygen sensor with LSF an dense diffusion barrier. *Key Engineering Materials* **336–338**, 417–419 (2007).
13. Toby, B. H. EXPGUI, a graphical user interface for GSAS. *J. Appl. Cryst.* **34**, 210–213 (2001).
14. Belous, A. G., Pashkova, E. V., Kravchyk, K. V., Ivanitskii, V. P. & V'yunov, O. I. Mossbauer and X-ray diffraction studies of cubic solid solutions of the ZrO_2-Y_2O_3-Fe_2O_3 system. *J. Phys. Chem. C* **112**, 3914–3919 (2008).
15. Guo, F. W. & Xiao, P. Effect of Fe_2O_3 doping on sintering of yttria-stabilized zirconia. *J. Eur. Ceram. Soc.* **32**, 4157–4164 (2012).
16. Satardekar, P., Montinaro, D. & Sglavo, V. M. Fe-doped YSZ electrolyte for the fabrication of metal supported-SOFC by co-sintering. *Ceram. Int.* **41**, 9806–9812 (2015).
17. Usui, T., Asada, A., Nakazawa, M. & Osanai, H. Gas polarographic oxygen sensor using an oxygen/zirconia electrolyte. *J. Electrochem. Soc.* **136**, 534–542 (1989).
18. Nagao, M. *et al*. Rechargeable metal-air proton-exchange membrane batteries for renewable energy storage. *ChemElectroChem* **3**, 247–255 (2016).
19. Kobayashi, K., Nagao, M. & Hibino, T. A rechargeable tinair PEM battery using $SnSO_4$ as an anode-active material. *Chem. Lett.* **45**, 161–163 (2016).
20. Wang, X. N., Liu, T., Wang, C. & Yu, J. K. Crystalline structure, microstructure and electrical characterizations of $FeO_{1.5}$ doped YSZ. *Ceram. Int.* **43**, 9577–9581 (2017).
21. Gao, X., Liu, T., Yu, J. K. & Li, L. Limiting current oxygen sensor based on $La_{0.8}Sr_{0.2}Ga_{0.8}Mg_{0.2}O_{3-\delta}$ as both dense diffusion barrier and solid electrolyte. *Ceram. Int.* **43**, 6329–6332 (2017).
22. Zhang, X. F. *et al*. A limiting current oxygen sensor with $La_{0.8}Sr_{0.2}(Ga_{0.8}Mg_{0.2})_{1-x}Fe_xO_{3-\delta}$ dense diffusion barrier. *J. Solid State Electrochem.* **21**, 1323–1328 (2017).
23. Gao, X., Liu, T., Zhang, X. F., He, B. G. & Yu, J. K. Properties of limiting current oxygen sensor with $La_{0.8}Sr_{0.2}Ga_{0.8}Mg_{0.2}O_{3-\delta}$ solid electrolyte and $La_{0.8}Sr_{0.2}(Ga_{0.8}Mg_{0.2})_{1-x}Cr_xO_{3-\delta}$ dense diffusion barrier. *Solid State Ion.* **304**, 135–144 (2017).
24. Han, J. X., Zhou, F., Bao, J. X., Wang, X. J. & Song, X. W. A high performance limiting current oxygen sensor with $Ce_{0.8}Sm_{0.2}O_{1.9}$ electrolyte and $La_{0.8}Sr_{0.2}Co_{0.8}Fe_{0.2}O_3$ diffusion barrier. *Electrochim. Acta* **108**, 763–768 (2013).
25. Gokcen, N. A. Vapor pressure of water above saturated lithium chloride solution. *J. Am. Chem. Soc.* **73**, 3789–3790 (1951).

Acknowledgements

This work is financially supported by the National Natural Science Foundation of China (51374055) and the Fundamental Research Funds for the Central Universities (N172506007).

Author Contributions

Xiangnan Wang conceived of the presented idea. X.N. Wang carried out the experiment and wrote the manuscript with support from T. Liu and Jingkun Yu. All authors discussed the results and contributed to the final manuscript.

Additional Information

Competing Interests: The authors declare no competing interests.

Publisher's note: Springer Nature remains neutral with regard to jurisdictional claims in published maps and institutional affiliations.